The ferro-antiferro bifurcation transition at the paraphase boundary in a microscopic model with incommensurate phases

1992 J. Phys. A: Math. Gen. 25 355

(http://iopscience.iop.org/0305-4470/25/2/016)

J. Phys. A: Math. Gen. 25 (1992) 355-365. Printed in the UK

The ferro–antiferro bifurcation transition at the paraphase boundary in a microscopic model with incommensurate phases

J S W Lamb†

Institute for Theoretical Physics, University of Nijmegen, Toernooiveld, 6525 ED Nijmegen, The Netherlands

Received 25 September 1991

Abstract. In a microscopic crystallographic model with incommensurate phases, the magnetoelastic DIFFOUR model, phase transitions at the paraphase boundary are connected to bifurcations of a symplectic mapping. Special attention is paid to the ferro-antiferro transition at the paraphase boundary and its implication on the incommensurate parts of the phase diagram. It is shown that the ferro-antiferro transition at the paraphase boundary is related to the crossing of a degenerate bifurcation point in the mapping. As such, the transition has been called a bifurcation transition.

1. Introduction

Over the past few decades, the study of incommensurate structures has led to the development of microscopic models that explain their occurrence. Well studied are the Frenkel-Kontorova (FK) model [1], the anisotropic (or axial) next-nearest-neighbour Ising (ANNNI) model [2] and the discrete frustrated ϕ^4 (DIFFOUR) model [3]. The search for ground states in these models has been related to symplectic mappings by Aubry and Le Daeron [4] for the FK model, by Høgh Jensen and Bak [5] for the ANNNI model and by Janssen and Tjon [6] for the DIFFOUR model.

This paper deals with the magnetoelastic DIFFOUR model, an extension of the DIFFOUR model. In section 2 the model is described. In section 3 a mapping, associated with the stationary condition, is introduced and in section 4 bifurcations of this mapping are related to the phase transitions at the paraphase boundary. In section 5 the phase diagrams of the magnetoelastic DIFFOUR model are presented. The ferro–antiferro bifurcation transition is then considered separately in section 6. Extended details have been put in the appendices.

2. The magnetoelastic DIFFOUR model

The magnetoelastic DIFFOUR model describes a chain of particles, embedded in a three-dimensional environment‡. The particles have a local ϕ^4 two-state spin character, through which they are coupled by harmonic next-nearest and magnetoelastic nearest-neighbour bonds. Furthermore, the particles are bound by ordinary harmonic springs.

† Present address: Institute for Theoretical Physics, University of Amsterdam, Valckenierstraat 65, 1018 XE Amsterdam, The Netherlands.

‡ One may think of the 'one-dimensional' interaction between uniformly organized stacked layers.

0305-4470/92/020355+11$04.50

The free energy at zero temperature ($T=0$) of such a chain is

$$F=\sum_n \frac{\alpha}{2}x_n^2+\frac{\gamma}{4}x_n^4+\frac{\beta_n}{2}(x_n-x_{n-1})^2+\frac{\delta}{2}(x_n-x_{n-2})^2+\frac{\kappa}{2}l_n^2+Pl_n \tag{1}$$

where x_n is the local spin variable and l_n is the stretching of the intermediate intervals between the successive particles with respect to some equilibrium distance. α and γ give shape to the local potential ($\alpha<0$ and $\gamma>0$), $\beta_n=\beta^{(0)}+\beta^{(1)}l_n$ is the (linear) magnetoelastic nearest neighbour and δ the harmonic next-nearest-neighbour coupling constant. κ is the strength of the interparticle bonds and P stands for the external pressure.

To obtain a phase diagram, we have to find the ground states (configurations with lowest energy) of the model. The ground states are among the stationary states which are found by the requirement that

$$\frac{\partial F}{\partial x_n}=0 \tag{2}$$

and

$$\frac{\partial F}{\partial l_n}=0. \tag{3}$$

From (3) we find that

$$l_n=-\frac{1}{\kappa}\left(\frac{\beta^{(1)}}{2}(x_n-x_{n-1})^2+P\right). \tag{4}$$

Substituting (4) in the expression, obtained from (2), we find that

$$\alpha x_n+\gamma x_n^3+\left(\beta^{(0)}-\beta^{(1)}\frac{P}{\kappa}\right)(2x_n-x_{n-1}-x_{n+1})+\delta(2x_n-x_{n-2}-x_{n+2})$$
$$+-\frac{\beta^{(1)2}}{2\kappa}[(x_n-x_{n-1})^3+(x_n-x_{n+1})^3]=0. \tag{5}$$

However, this is just the stationary condition following from the effective free energy

$$F_{\text{eff}}=\sum_n\left\{\frac{\alpha}{2}x_n^2+\frac{\gamma}{4}x_n^4+\frac{\beta}{2}(x_n-x_{n-1})^2+\frac{\varepsilon}{4}(x_n-x_{n-1})^4+\frac{\delta}{2}(x_n-x_{n-2})^2\right\} \tag{6}$$

with

$$\varepsilon=-\frac{\beta^{(1)2}}{2\kappa} \quad \text{and} \quad \beta=\beta^{(0)}-\beta^{(1)}\frac{P}{\kappa}. \tag{7}$$

We observe that β takes account of the pressure and ε of the magnetoelastic coupling. The original DIFFOUR potential equals F_{eff} if the magnetoelastic coupling is turned off ($\beta^{(1)}=0$), as it should.

Furthermore, it turns out that, since ε is strictly negative, the magnetoelastic coupling tends to destabilize the chain. If $\varepsilon<-\gamma/16$ the free energy has no lower bound and hence the model has no stable ground state.

To study the model at non-zero temperatures we use a mean field argument [3] to modify (6): averaging the equation of motion gives

$$-m\langle\ddot{x}_n\rangle = \alpha\langle x_n\rangle + \gamma\langle x_n^3\rangle + \beta(2\langle x_n\rangle - \langle x_{n-1}\rangle - \langle x_{n+1}\rangle)$$
$$+ \varepsilon[\langle(x_n - x_{n-1})^3\rangle + \langle(x_n - x_{n+1})^3\rangle] + \delta(2\langle x_n\rangle - \langle x_{n-2}\rangle - \langle x_{n+2}\rangle). \tag{8}$$

Under the assumption that $\langle x_n^2 x_m\rangle \simeq \langle x_n^2\rangle\langle x_m\rangle$ and that the thermal fluctuations do not depend on n, we find that

$$\langle(x_n - x_{n-1})^3\rangle + \langle(x_n - x_{n+1})^3\rangle$$
$$\simeq \langle x_n - x_{n-1}\rangle^3 + \langle x_n - x_{n+1}\rangle^3 + 4(\langle x_n^2\rangle - \langle x_n\rangle^2)(2\langle x_n\rangle - \langle x_{n-1}\rangle - \langle x_{n+1}\rangle)$$

$$\langle x_n^3\rangle \simeq \langle x_n^2\rangle\langle x_n\rangle = \langle x_n\rangle^3 + (\langle x_n^2\rangle - \langle x_n\rangle^2)\langle x_n\rangle.$$

Hence we may account for temperature in the following way

$$\alpha \mapsto \alpha + \gamma T \qquad \beta \mapsto \beta + 4\varepsilon T \tag{9}$$

where $T = (\langle x_n^2\rangle - \langle x_n\rangle^2)$ is a measure of the thermal fluctuations, i.e. temperature (in appropriate units)†.

3. The mapping

The stationary condition (5) can be written, accounting for temperature by (9), as

$$x_{n+2} = \frac{\alpha + \gamma T}{\delta} + \frac{\gamma}{\delta} x_n^3 + \frac{\beta + 4\varepsilon T}{\delta}(2x_n - x_{n+1} - x_{n-1})$$
$$+ \frac{\varepsilon}{\delta}[(x_n - x_{n-1})^3 + (x_n - x_{n+1})^3] + 2x_n - x_{n-2}. \tag{10}$$

We may look at (10) as a four-dimensional mapping

$$M: \begin{pmatrix} x_{n+1} \\ x_n \\ x_{n-1} \\ x_{n-2} \end{pmatrix} \mapsto \begin{pmatrix} x_{n+2} \\ x_{n+1} \\ x_n \\ x_{n-1} \end{pmatrix}. \tag{11}$$

Application of M to an arbitrary starting configuration of four points produces a unique continuation of the chain as a stationary configuration. One should recognize, however, that these stationary configurations do not have to be ground states; in fact most of them are not.

The linearized mapping has the following form

$$\mathrm{d}M = \begin{pmatrix} B & A & B & -1 \\ 1 & 0 & 0 & 0 \\ 0 & 1 & 0 & 0 \\ 0 & 0 & 1 & 0 \end{pmatrix} \tag{12}$$

† In this approximation, we assume that the fluctuations of l_n are coupled strongly to the fluctuations of x_n.

where at the paraphase ($x_n = 0$ for all n)

$$A = \frac{\alpha + 2\beta + 2\delta + (\gamma + 8\varepsilon)T}{\delta} \tag{13}$$

$$B = -\frac{\beta + 4\varepsilon T}{\delta}. \tag{14}$$

From (12) it can be concluded immediately that the mapping is symplectic and hence that the eigenvalues of the linearized mapping come in pairs or four-tuples (if λ is an eigenvalue, λ^* and λ^{-1} are also eigenvalues) [6].

The bifurcations of this mapping have been studied thoroughly [6, 7] and it is known that a bifurcation to a structure with modulation vector q occurs as a pair of eigenvalues collides on the unit circle at $\exp(iq)$. For instance, if the eigenvalues collide at $q = \pi$, the bifurcation is period-doubling and if the collision occurs at $q = 0$, there is a period preserving bifurcation.

4. Phase transitions at the paraphase boundary

The paraphase is the phase with $x_n = 0$ for all n. From the ϕ^4 character of the energy it follows directly that the only way in which there can be a phase transition, is in a smooth way, i.e. there are only second-order phase transitions at the paraphase boundary. Hence at the paraphase boundary, the paraphase has to be marginally stable.

Janssen and Tjon [6] related second-order phase transitions to bifurcations in the symplectic mapping. They found that if the linearized mapping has an eigenvalue λ on the complex unit circle, the configuration is marginally stable in the direction of the eigenvector. A proof of this proposition is stated in appendix A.

The symplecticity of the mapping leaves no other possibility than that the second-order phase transitions at the paraphase boundary occur simultaneously with a collision of eigenvalues of the linearized mapping at the unit circle. This is in fact what happens: a collision of eigenvalues on the unit circle at $\exp(iq)$ corresponds to a soft mode with wavevector q.

5. Phase diagrams

By an analysis similar to the one of Janssen and Tjon [3], using the mapping to find the exact phase boundaries for the paraphase (see appendix B) and numerical calculations to study the other phases, some phase diagrams have been constructed†. The phases $\langle n \rangle$ in the figures correspond for n even to a phase with a periodic continuation of respectively $n/2$ 'spins up' ($x_n > 0$) and $n/2$ 'spins down' ($x_n < 0$), and for odd n to a phase with a periodic continuation of respectively $(n+1)/2$ 'spins up' and $(n-1)/2$ 'spins down'.

In figure 1 the $T = 0$ phase diagram is depicted. In the neighbourhood of the point $\beta = \delta = 0$ the diagram seems to exhibit a multiphase point. This is not the case, however.

† By a proper gauge in all calculations α and γ have been fixed to $\alpha = -\gamma = -1$. The magnetoelastic coupling in all calculations has been chosen as $\varepsilon = -\frac{1}{32}$, right in the middle of the allowed interval $\langle -\frac{1}{16}, 0]$, as a proper representant of the magnetoelastic case.

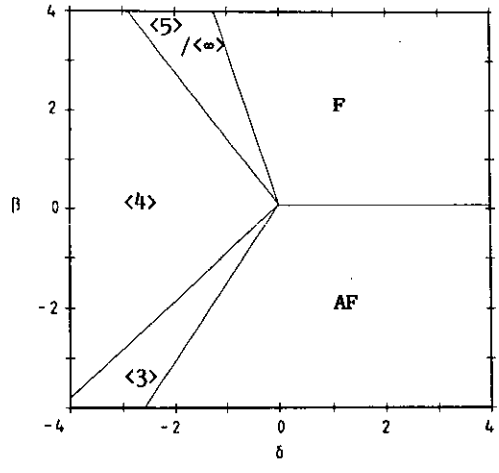

Figure 1. $T=0$ phase diagram of the magnetoelastic DIFFOUR model ($\varepsilon=-\frac{1}{32}$). The region $\langle 5\rangle/\langle\infty\rangle$ contains a fan of phases from $\langle 5\rangle$ to $\langle\infty\rangle$.

It is just the remnant of the multiphase point that does exist in the original DIFFOUR model ($\varepsilon=0$)†.

It turns out that the $\delta<0$ part of parameter space is the interesting part with incommensurate phases. If $\delta>0$, the β–T phase diagram (that may be interpreted as the P–T diagram) consists of just three regions: a para, a ferro and an antiferro phase.

In figure 2 the β–T phase diagram (that may be interpreted as the P–T diagram) (with $\delta=-\frac{1}{2}$) is presented. One can distinguish four regions: a para phase, a ferro phase, an antiferro phase and a region with higher commensurate and incommensurate phases. It shows much resemblance to the phase diagram of the DIFFOUR model ([8],

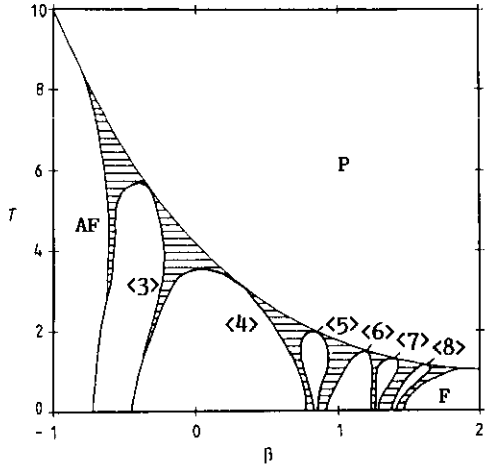

Figure 2. β–T diagram of the magnetoelastic DIFFOUR model ($\delta=-\frac{1}{2}$, $\varepsilon=-\frac{1}{32}$). The hatched regions contain intermediate phases.

† If $\varepsilon=0$, the energy at $\beta=\delta=0$ is given by $v=\sum_n -\frac{1}{2}x_n^2+\frac{1}{4}x_n^4$ and the ground state is degenerate: all configuration with particles at positions 1 or -1 have the same energy density $v=-\frac{1}{4}$. If $\varepsilon\neq 0$ this multiphase point is destroyed.

figure 10). This is not surprising, since the magnitude of the magnetoelastic coupling is very small.

6. The ferro–antiferro bifurcation transition

A picture that is totally different from figure 2 is obtained if one considers a δ–T section through parameter space.

The stability boundaries of the para, ferro and antiferro phase have been calculated explicitly (see appendix B). For three different values of β the stability boundaries of these phases have been drawn in the δ–T diagram in figure 3.

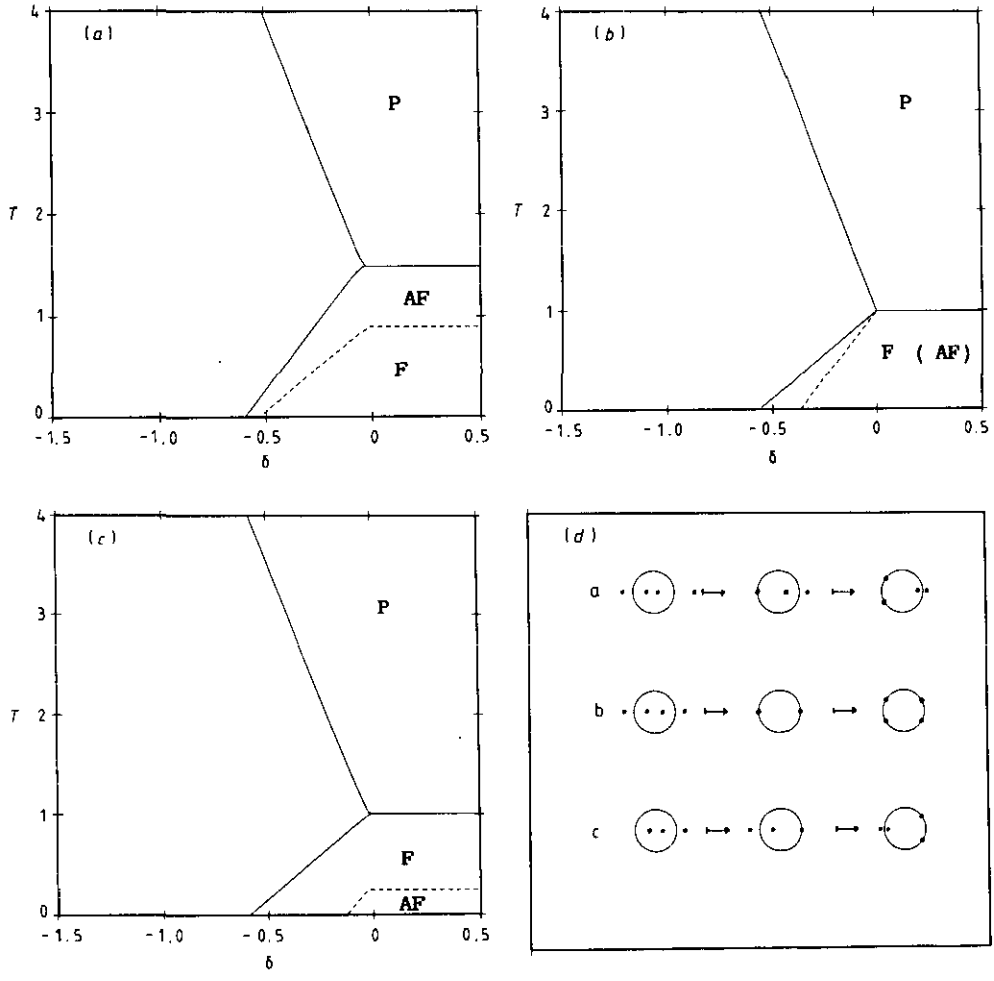

Figure 3. Stability boundaries of the para (P), ferro (F) and antiferro (AF) phase (dashed lines denote boundaries of metastable states) (*a*) before the bifurcation transition ($\varepsilon = -1/32, \beta = 1/16$), (*b*) at the bifurcation transition ($\varepsilon = -1/32, \beta = 1/8$) (the AF phase is metastable), (*c*) after the bifurcation transition ($\varepsilon = -1/32, \beta = 3/16$); (*d*) the behaviour of the eigenvalues of the linearized mapping (from the point of view of the para phase) around the phase transition (at $\delta > 0$) in complex plane is illustrated, following a path of decreasing temperature.

Two different regimes are distinguished:

$\beta < \frac{1}{8}$: the antiferro phase borders the para phase

$\beta > \frac{1}{8}$: the ferro phase borders the para phase.

In between the two regimes, if $\beta = \frac{1}{8}$, the situation is degenerate.

To observe what happens, the behaviour of the eigenvalues of the linearized mapping (from the point of view of the para phase) around the phase transition (at $\delta > 0$) has been illustrated, following a path of decreasing temperature.

Above the phase transition, the four eigenvalues are on the real axis, two of them on the positive and two on the negative side. As temperature is decreased, the eigenvalues approach the unit circle. The actual type of phase transition is determined by whether the positive or the negative eigenvalues reach the unit circle first. If the positive eigenvalues reach the unit circle first, there is a para–ferro transition, otherwise the para phase borders the antiferro phase.

At the bifurcation transition, both pairs of eigenvalues arrive at the unit circle at the same instant and the period-doubling bifurcation occurs simultaneously with the

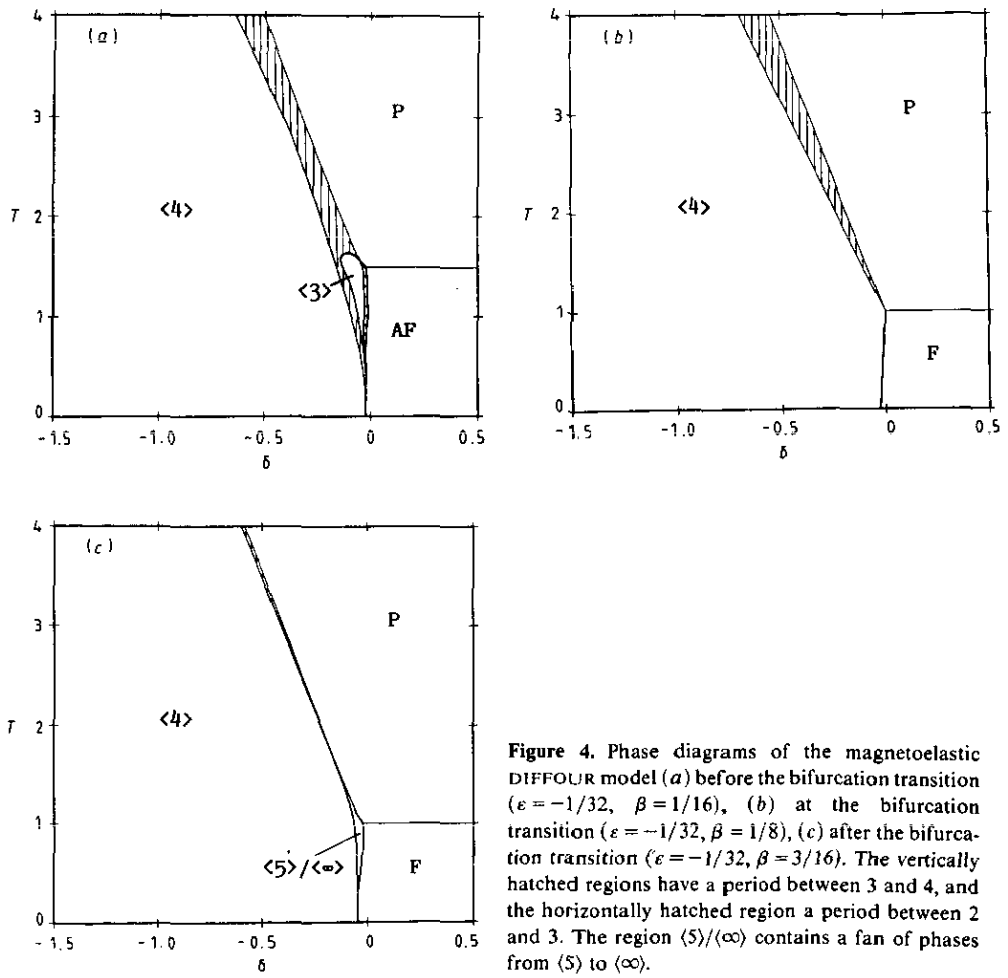

Figure 4. Phase diagrams of the magnetoelastic DIFFOUR model (*a*) before the bifurcation transition ($\varepsilon = -1/32$, $\beta = 1/16$), (*b*) at the bifurcation transition ($\varepsilon = -1/32$, $\beta = 1/8$), (*c*) after the bifurcation transition ($\varepsilon = -1/32$, $\beta = 3/16$). The vertically hatched regions have a period between 3 and 4, and the horizontally hatched region a period between 2 and 3. The region $\langle 5\rangle/\langle\infty\rangle$ contains a fan of phases from $\langle 5\rangle$ to $\langle\infty\rangle$.

period preserving bifurcation. Such a degenerate bifurcation occurs each time if

$$\beta = -4\varepsilon. \tag{15}$$

We can characterize the bifurcation transition by a special wavevector

$$q_{BT} = \cos^{-1}\left(\frac{8\varepsilon + 1 - \sqrt{16\varepsilon + 1}}{8\varepsilon}\right). \tag{16}$$

Before the bifurcation transition, if $\beta < -4\varepsilon$, the paraphase boundary with varying soft mode wavevector has wavevectors in the interval $\langle q_{BT}, \pi]$ and afterwards, if $\beta > -4\varepsilon$, in the interval $[0, q_{BT}\rangle$.

At the bifurcation transition, the paraphase boundary with varying soft mode vector is replaced, for an instant, by a (straight) boundary with a constant soft mode vector: q_{BT}. The point $\delta = T = 0$ becomes at the bifurcation transition soft for all $q \in [0, \pi]$. The corresponding dispersion curve at that point is flat zero.

It follows directly from (16) that $q_{BT} \in [\pi/2, \pi\rangle$. It is furthermore remarkable that the type of bifurcation depends solely on the strength of the magnetoelastic coupling.

The impact of the occurence of the bifurcation transition on the other phases is investigated by numerical calculations. The resulting phase diagrams are presented in figure 4 (for $\varepsilon = -\frac{1}{32}$, $q_{BT} = 1.74\ldots$). They show that, around the bifurcation transition, the incommensurate phases are trapped between the para and (anti)ferro phase on one side and the $\langle 4\rangle$ phase on the other side. It is in that region that side effects of the bifurcation transition are observed.

7. Concluding remarks

It has been shown that the extension of the DIFFOUR model to the magnetoelastic DIFFOUR model displays, despite the small allowed magnetoelastic coupling, a non-trivial bifurcation transition. In fact, the bifurcation transition also occurs in the DIFFOUR model, since it is just the case $\varepsilon = 0$. However, the characterizing vector q_{BT} then is fixed to $\pi/2$ (corresponding to a soft mode transition to the $\langle 4\rangle$ phase) and hence the transition is of less importance to the incommensurate phases.

The connection of the phase transitions at the paraphase boundary with the bifurcations of a four-dimensional symplectic mapping has shown to provide an effective means of illustrating the ferro-antiferro bifurcation transition.

It should be noted that the account for temperature in the effective free energy (6) is only correct up to fourth order. A proper account of temperature requires true mean field calculations that give, however, less insight in the phase transition mechanism. It has been shown by Janssen and Tjon [9] for the DIFFOUR model that the results of true mean field calculations are in good qualitative agreement with the results, obtained by the effective mean field argument that has been used in this paper.

Acknowledgment

I am grateful to T Janssen for many stimulating discussions on the subject and for using one of his computer programs.

Appendix A. Relation between bifurcations and phase transitions

Proposition (Janssen and Tjon [6]). For systems with free energy $F(\{u_i\})$, fixed points of the related mapping problem that have eigenvalues of the linearized mapping on the complex unit circle are at most marginally stable configurations.

Proof. Consider the dispersion curves $\omega^2(q)$ of a configuration with period p. They are the eigenvalues of the dynamical matrix

$$D_{ij} = \frac{\partial^2 F}{\partial u_i \partial u_j}\bigg|_u . \tag{17}$$

The eigenvalue equation thus reads

$$D_{ij}\varepsilon_j = \omega^2 \varepsilon_i \tag{18}$$

where $\boldsymbol{\varepsilon}$ is an eigenvibration vector. By Fourier transformation, using the periodicity, we obtain a more convenient expression, writing $j = np + m$ and $i = n'p + m'$,

$$\varepsilon_j = \varepsilon_{np+m} = \int_0^{2\pi} \varepsilon_m^{(q)} \, \mathrm{e}^{\mathrm{i}qn} \, \mathrm{d}q \tag{19}$$

$$\Rightarrow \sum_{n,m} \frac{\partial^2 F}{\partial u_{n'p+m'} \partial u_{np+m}}\bigg|_u \varepsilon_m^{(q)} \, \mathrm{e}^{\mathrm{i}qn} = \omega^2(q) \varepsilon_{m'}^{(q)} \, \mathrm{e}^{\mathrm{i}qn'} . \tag{20}$$

The mapping that is used, is obtained by requiring stationarity

$$\frac{\partial F}{\partial u_i} = 0 \tag{21}$$

and hence its linearized form is given (implicitly) by

$$\sum_j \frac{\partial^2 F}{\partial u_i \partial u_j}\bigg|_u \varepsilon_j = 0. \tag{22}$$

An eigenvector of the linearized mapping with some eigenvalue λ, is an orbit with the following property:

$$\varepsilon_j = \varepsilon_{np+m} = \varepsilon_m \cdot \lambda^n . \tag{23}$$

And for the eigenvector, (22) reads

$$\sum_{n,m} \frac{\partial^2 F}{\partial u_{n'p+m'} \partial u_{np+m}}\bigg|_u \varepsilon_m \lambda^n = 0. \tag{24}$$

If λ in (24) equals $\mathrm{e}^{\mathrm{i}q}$ then we may identify ε_m as $\varepsilon_m^{(q)}$ and we find that $\omega^2(q) = 0$, i.e. *a soft mode with wavevector q, since (20) has to hold for all n' and m'.* □

Appendix B. Explicitly calculated stability boundaries

For the paraphase (P), the ferrophase (F) and the antiferrophase (AF) the stability regions have been calculated explicitly, regarding the vibration spectra.

By Fourier transformation we find from the dynamical equation for the paraphase (P) and the ferrophase (F) that

$$m\omega^2(q) = \alpha + \gamma T + 3\gamma\bar{x}^2 + 4(\beta + 4\varepsilon T)\sin^2\left(\frac{q}{2}\right) + 4\delta\sin^2(q) \tag{25}$$

and for the antiferrophase (AF) ($|x_n| = B$) that

$$m\omega^2(q) = \alpha + \gamma T + 3\gamma B^2 + 4\delta\sin^2\left(\frac{q}{2}\right) + (2(\beta + 4\varepsilon T) + 24\varepsilon B^2)\left(1 \pm \cos\left(\frac{q}{2}\right)\right). \tag{26}$$

The configurations, their energy density v and their stability boundaries with corresponding soft mode wavevector (under the gauge $-\alpha = \gamma = 1$) are presented in table 1.

Table 1. Explicitly calculated stability boundaries.

(P)	$x_n = 0$ $\mathcal{V} = 0$
soft mode	stability boundary
$q = 0$	$T = 1$
$q = \pi$	$T = (1 - 4\beta)/(16\varepsilon + 1)$
$\cos(q) = -(\beta + 4\varepsilon T)/(4\delta)$	$-1 + T + 2\beta + 8\varepsilon T + 4\delta + (\beta + 4\varepsilon T)^2/(4\delta) = 0$
(F)	$x_n = (1 - T)^{1/2}$ $\mathcal{V} = -\dfrac{(1 - T)^2}{4}$
soft mode	stability boundary
$q = 0$	$T = 1$
$q = \pi$	$T = \dfrac{1 + 2\beta}{1 - 8\varepsilon}$
$\cos(q) = -(\beta + 4\varepsilon T)/(4\delta)$	$2 + (8\varepsilon - 2)T + 2\beta + 4\delta + (\beta + 4\varepsilon T)^2/(4\delta) = 0$
(AF)	$x_n = (-)^n\left(\dfrac{1 - 4\beta}{16\varepsilon + \gamma} - T\right)^{1/2}$ $\mathcal{V} = -\dfrac{(T(16\varepsilon + 1) + 4\beta - 1)^2}{4(16\varepsilon + 1)}$
soft mode	stability boundary
$q_1 = 0,\ q_2 = \pi$	$T = -\dfrac{1}{2} + \dfrac{3}{2}\left(\dfrac{1 - 4\beta}{1 + 16\varepsilon}\right)$
$q_1 = \pi,\ q_2 = 0$	$T = \dfrac{1 - 4\beta}{1 + 16\varepsilon}$
$\cos(q_1) = -\cos(q_2)$	$T - 1 + 2(\beta + 4\varepsilon T) + (3 + 24\varepsilon)\left[\dfrac{1 - 4\beta}{16\varepsilon + 1} - T\right]$
$\ldots = -\left(\beta + 4\varepsilon\left(3\left[\dfrac{1 - 4\beta}{16\varepsilon + 1}\right] - 2T\right)\right)\Big/(4\delta)$	$+ 4\delta + \left(\beta + 4\varepsilon\left(3\left[\dfrac{1 - 4\beta}{16\varepsilon + 1}\right] - 2T\right)\right)^2\Big/(4\delta) = 0$

References

[1] Frenkel Y I and Kontorova T 1938 *Zh. Eksp. Teor. Fiz.* **8** 1340
[2] Selke W 1988 *Phys. Rep.* **170** 213
[3] Janssen T and Tjon J A 1982 *Phys. Rev.* B **25**(4) 3767
[4] Aubry S and Le Daeron P Y 1983 *Physica* **8D** 381
[5] Høgh Jensen M and Bak P 1983 *Phys. Rev.* B **27** 6853
[6] Janssen T and Tjon J A 1983 *J. Phys. A: Math. Gen.* **16** 673
[7] Hu B and Mao J 1987 *Directions in Chaos* **1** (*World Scientific Series on Directions in Condensed Matter Physics* **3**) (Singapore: World Scientific) p 206
[8] Currat R and Janssen T 1983 *Solid State Physics* **41** (San Diego: Academic) 202
[9] Janssen T and Tjon J A 1983 *J. Phys. C: Solid State Phys.* **16** 4789